# Feedback Tolerant Quantum Dot Lasers Integrated With 300 mm Silicon Photonics

Duanni Huang, Xinru Wu, Shane Yerkes, Guan-Lin Su, Karan Mehta, Marcus Cramer, Stan Dobek, Chelsea Mackos, Timothy Ward, Pari Patel, Ranjeet Kumar, Songtao Liu, Xiaoxi Wang, Junyi Gao, Mark Isenberger, Harel Frish, and Haisheng Rong, *Fellow, IEEE*

*(Top-Scored Paper)*

***Abstract*—We report on the first quantum dot lasers heterogeneously integrated with 300 mm silicon photonics. The lasers show linewidth enhancement factor near zero, indicating the capability for high feedback tolerance, which enables isolator-free operation. We demonstrate this concept by using a heterogeneous III-V/Si quantum dot laser with a silicon microring modulator in the presence of optical feedback of up to −13 dB without degradation to eye quality for a 128 Gb/s PAM-4 signal.**

***Index Terms*—Lasers, quantum dots, silicon integrated photonics.**

## I. Introduction

QUANTUM dot (QD) lasers have many claimed benefits over more commonly used quantum well lasers such as lower threshold current density, higher gain at elevated temperatures, reduced gain competition enabling multi-wavelength operation, and a high tolerance for optical feedback due to a low linewidth enhancement factor [1], [2], [3]. Among these many benefits, the reduced sensitivity to optical reflections has spurred the interest of many researchers lately due to the potential to realize optical isolator free operation [4], [5]. Optical isolators are typically required to protect the laser from spurious back-reflections in most real-world applications but are extremely challenging to integrate with lasers as a part of a photonic integrated circuit (PIC) due to material incompatibility and high insertion losses [6], [7]. As a result, optical isolators have remained a discrete photonic component, only interfacing with the PIC through packaging and assembly. Removing the need for optical isolators by using feedback insensitive QD lasers is greatly desired as it would significantly reduce the packaging and assembly cost and complexity.

While there has been tremendous progress in recent years to improve the performance of QD lasers, most demonstrations have focused on standalone lasers rather than photonic integration to form the highly complex photonic integrated circuits (PICs) needed for transceivers. Heterogeneous integration of quantum dot gain materials with silicon photonics allows us to realize the benefits of QD lasers as well as utilize the rich library of silicon photonic waveguide devices. Furthermore, integration with silicon enables scaling to a 300 mm process, allowing for advanced lithography capabilities in 300 mm CMOS fabs and the potential to scale QD technology to very high volume and throughput. Previous works enabling QDs on 300 mm wafers have focused on monolithic growth of QDs on silicon [8], [9]. These approaches require thick buffer layers between the QDs and silicon substrate or growth in patterned pockets in the silicon, resulting in limited coupling of light from the laser to a silicon waveguide [10]. Other recent QD works demonstrate coupling to silicon waveguides but are at a smaller wafer scale [11], [12]. In this work, we demonstrate, to the best of our knowledge, the first heterogeneously integrated silicon QD lasers on a 300 mm silicon photonics platform with coupling to silicon waveguide devices. We demonstrate QD Fabry-Perot lasers lasing up to 150 °C, as well as DFB lasers with >28 mW of output power and resiliency to optical feedback up to −13 dB.

## II. Quantum Dot Laser Design and Fabrication

The heterogeneously integrated quantum dot laser on silicon has many similarities to Intel's heterogeneously integrated quantum well lasers that are in high-volume production today [13], [14]. Therefore, the general design philosophy is similar as well. Multi-stage adiabatic tapers are used to transition the light from a purely passive silicon waveguide into a hybrid silicon/III-V mode that serves as the optical gain waveguide. The optical confinement in the active region can be tailored by changing the silicon waveguide width. The silicon layer directly under the III-V material can also be patterned with waveguide Bragg gratings with high precision on the pitch and grating strength for DFB lasers, which is enabled by 300 mm CMOS lithography [15]. Alternatively, the cavity mirrors for the laser can be placed outside of the III-V areas. This approach has been previously demonstrated with heterogeneously integrated QD tunable lasers and mode-locked lasers [16], [17]. The design flexibility enabled by heterogeneous III-V on silicon integration has been thoroughly explored with quantum well materials [18], and largely carries over to quantum dot gain materials as well.

Received 29 August 2024; revised 3 October 2024; accepted 7 October 2024. Date of publication 16 October 2024; date of current version 17 February 2025. *(Corresponding author: Duanni Huang.)*

The authors are with Intel Corporation, Santa Clara, CA 95054 USA (e-mail: duanni.huang@intel.com).

Color versions of one or more figures in this article are available at https://doi.org/10.1109/JLT.2024.3481454.

Digital Object Identifier 10.1109/JLT.2024.3481454

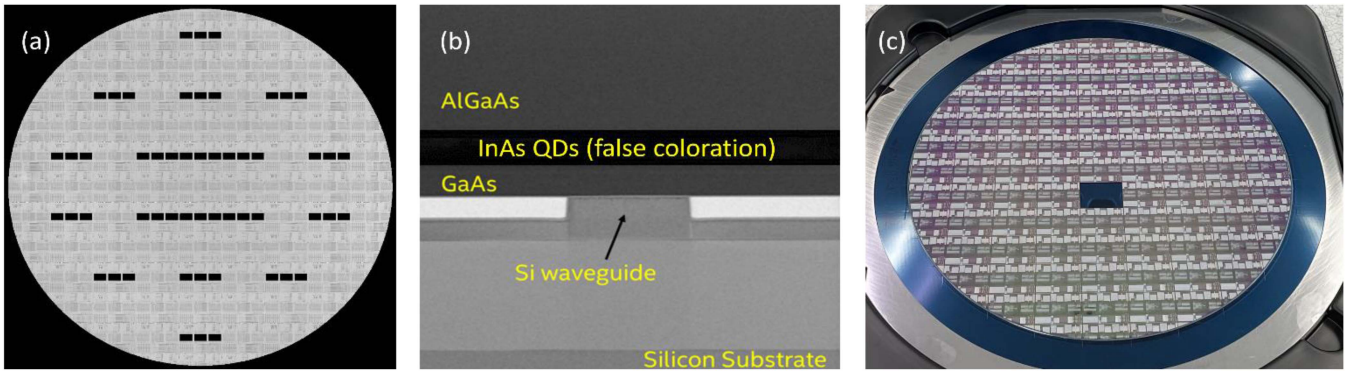


Fig. 1. (a) A 300 mm SOI wafer with 54 QD die (dark rectangles) bonded on it. (b) Cross-section of the hybrid silicon QD laser with active region and silicon waveguide. (c) Picture of the wafer at end of line. One die was removed for additional testing.

The heterogeneous silicon/III-V fabrication process begins with a 300 mm SOI wafer. The silicon device layer is patterned with waveguides, MMIs, directional couplers, and gratings needed to form the laser cavities. It also contains grating couplers to couple light in and out of the silicon waveguides, and doped silicon regions needed for p-i-n silicon variable optical attenuators, heaters, and modulators. All silicon patterning is carried out with DUV lithography, which is well suited for high-volume CMOS manufacturing.

Next, the InAs/GaAs quantum dot epitaxial wafer is diced into small dies in preparation for bonding. All the QD dies are bonded onto the SOI wafer as shown in Fig. 1(a) using direct plasma-activated bonding. For this wafer, a sparse bonding map containing 54 GaAs dies was used. A cross-section of the QD epi bonded on top of a silicon waveguide is shown in Fig. 1(b). After substrate removal of the bulk GaAs, the remaining epitaxial layers are patterned using a combination of dry and wet etches to form the laser mesas and tapers between the active laser waveguide and the passive silicon waveguides. By defining the tapers after bonding, the tapers are lithographically aligned with the silicon waveguides. Finally, contact metals are deposited and patterned for the laser and the underlying silicon devices. Images of a finished 300 mm wafer are shown in Fig. 1(c).

## III. Laser Characterization

### A. Fabry-Perot QD Laser

Fabry-Perot (FP) lasers with a 500 $\mu$m long gain section are formed with a high (R $\sim$ 100%) and partial (R $\sim$ 40%) reflectivity loop mirror as shown in Fig. 2(a). Due to the length of tapers, MMIs, and general waveguide routing, the total cavity length including the loop mirrors is roughly 1500 $\mu$m. The output light emitted from the partial 40% reflector exits the chip through a grating coupler (GC) and is measured using a broad-area photodetector after calibrating for coupling losses. The QD-FP laser is tested under different stage temperatures ranging from 30 °C to 150 °C and the results are plotted in Fig. 2(b). The threshold current is 20 mA at 30 °C and increases to 40 mA at 110 °C corresponding to a characteristic temperature $T_0$ of 115 °C in this range. Meanwhile, the output power of the laser only drops by 0.7 dB between 30 °C and 110 °C, demonstrating

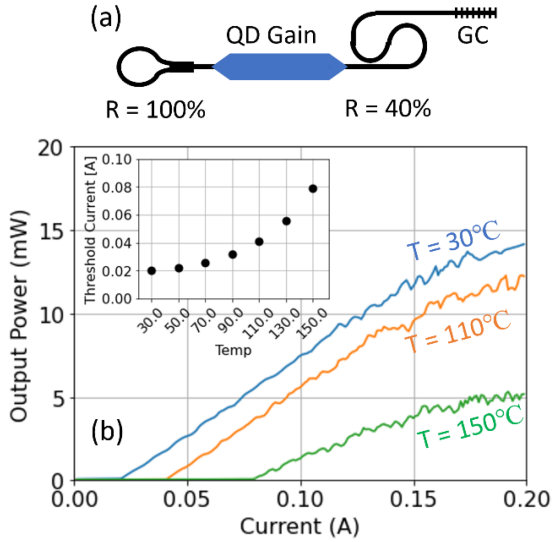


Fig. 2. (a) Schematic of the QD-FP laser with integrated loop mirrors fabricated from silicon waveguides. (b) The L-I curves of the FP laser up to 150 °C. The threshold currents are plotted in the inset.

the superior temperature ability of the QDs. Past 110 °C, the laser threshold increases, and the output power drops more rapidly, but it still shows clear signatures of lasing at 150 °C with >5 mW of output power.

Next, the QD-FP laser is studied at continuous wave conditions just below the 20 mA threshold current to observe the amplified spontaneous emission (ASE) of the device, which can be used to determine the linewidth enhancement factor (LEF), or alpha factor ($\alpha$). The ASE is collected for bias currents between 10 and 20 mA beyond which the laser begins to lase. One snapshot is shown in Fig. 3(a). The ASE ripples, a signature of the FP cavity, do not blueshift with increasing current, which indicates that the real part of the modal refractive index is not changing with increased current density. After using the Hakki-Paoli method [19] to obtain the differential gain, we calculate the LEF to be nearly zero between 1280 and 1320 nm in Fig. 3(b). At some wavelengths, the extracted value is slightly negative, which we attribute to the slight redshift in the ASE ripples due to the Joule heating of the laser as well as the limited resolution of

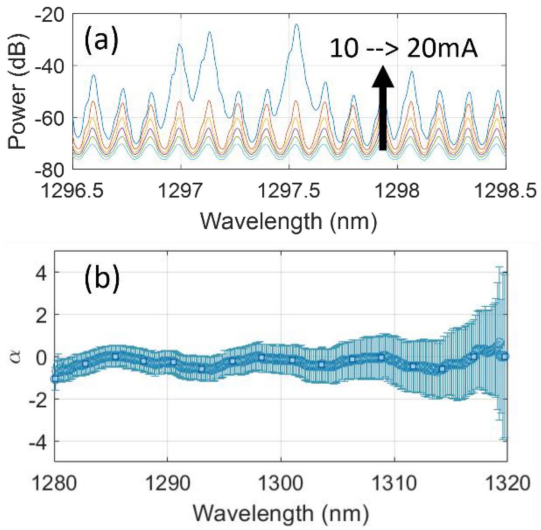


Fig. 3. (a) The amplified spontaneous emission of the QD-FP laser for different subthreshold bias currents. (b) The linewidth enhancement factor, or alpha factor extracted from the measurements in (a). An error bar representing the limitations of the optical spectrum analyzer resolution is overlaid on the data.

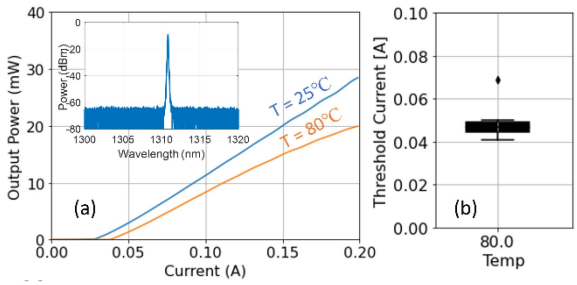


Fig. 4. (a) L-I curve for a quantum dot DFB laser at 25 and 80 °C. The inset shows single-mode emission near 1310 nm. (b) Threshold current statistics for the same QD-DFB design collected across the 300 mm wafer at 80 °C.

the optical spectrum analyzer. This near-zero LEF matches other predictions and experimental demonstrations of QD lasers in the literature [20], [21], [22] and is significantly improved over that of typical QW lasers (∼2 to 5) [23]. Measurements outside of this wavelength range are limited due to the spectral bandwidth limitations of the grating coupler. The near-zero LEF implies that the laser should not enter coherence collapse until very high levels of optical feedback, due to the $(1+\alpha^2)/\alpha^4$ dependence of the critical feedback level on $\alpha$ [24]. This is further explored in Section IV.

### B. DFB Laser

For stable single-wavelength operation with high output power, DFBs are generally the preferred choice for many real-world applications. At room temperature, the 1-mm long QD-DFB lasing near 1310 nm in Fig. 4(a) has a threshold of 26 mA and 28 mW of measured output power (double-sided) at 200 mA of drive current. The output power drops by 1.5 dB to 20 mW and the threshold current increases to 42 mA at 80 °C. The SMSR of the laser is over 50 dB and does not change with temperature. The L-I curves are very smooth, indicating that there is little to no

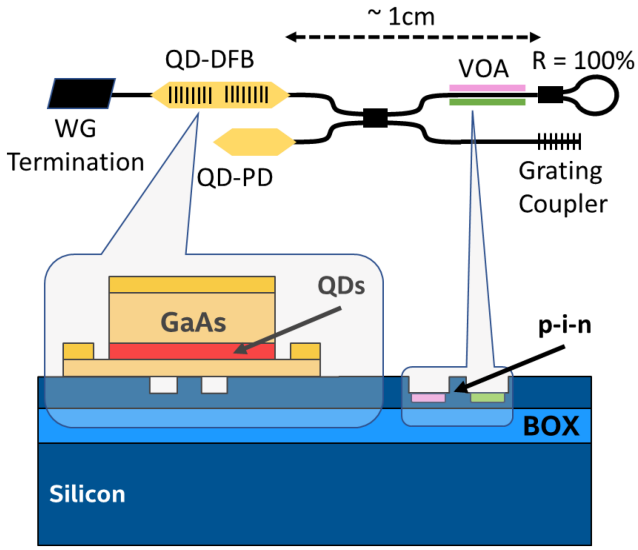


Fig. 5. Schematic of the heterogeneous silicon QD-DFB laser with integrated on-chip optical feedback tolerance test PIC. The black lines represent silicon waveguides, while the pink and green areas represent doped silicon regions.

mode-hopping occurring throughout the sweep of bias current. The device under test is representative of a typical QD-DFB laser on the wafer, as shown by the tight threshold current distribution across an entire wafer in Fig. 4(b).

The reduction in optical power at high temperatures is higher for the QD-DFB compared to the QD-FP laser since the laser wavelength is fixed by the Bragg wavelength, which walks off from the gain peak with increasing temperature. Control of the lasing wavelength and its detuning from the gain peak is important to achieve high-performing lasers across a wide temperature range in a high-volume manufacturing environment. Defining the laser grating in silicon in a CMOS fab allows for additional design flexibility and excellent repeatability in lasing wavelength [25]. This will result in high repeatability in laser performance and overall higher yields.

## IV. Feedback Tolerance Study

### A. QD-DFB RIN Versus Optical Feedback

To quantify the optical feedback tolerance of the heterogeneous QD on silicon laser, a QD-DFB lasing near its gain peak at 1300 nm is placed in the on-chip testbed shown in Fig. 5. One crucial benefit of integrating the QD laser with silicon photonics is the capability to add on-chip power monitors, power splitters, reflectors, and attenuators, enabling a fully on-chip optical feedback testbed. The QD-DFB is input into a 2 × 2 MMI with 50:50 splitting ratio. One output of the 2 × 2 MMI is connected to a silicon p-i-n doped variable optical attenuator (VOA) and a high-reflectivity loop mirror. The loop mirror consists of a 1 × 2 MMI with the outputs connected to each other and provides > 92% reflection. The round-trip optical loss through the VOA and loop mirror ranges from −7 dB to −24 dB, as measured by the on-chip QD photodetector and also verified using passive test structures. Combined with the 3 dB splitting loss (6 dB round trip) through the 2 × 2 MMI, the

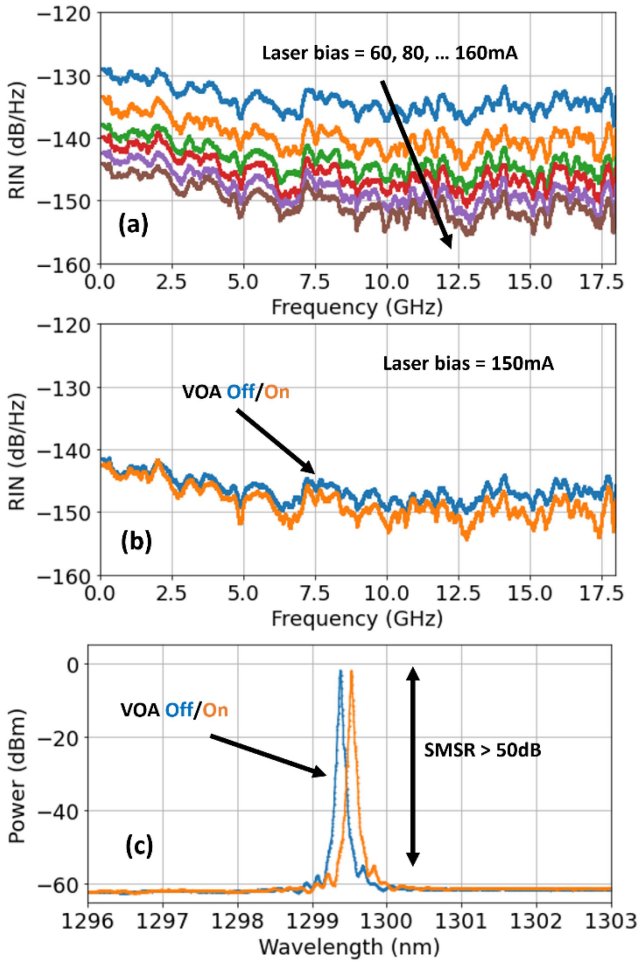


Fig. 6. (a) RIN of the QD-DFB laser at different laser bias currents. (b) The RIN and (c) optical spectrum of the QD-DFB with the VOA on (−30 dB backreflection) and off (−13 dB backreflection). All measurements are taken at room temperature.

total optical backreflection going back into the QD-DFB ranges from −13 dB to −30 dB, which is a typical range of values for reflection levels from on-chip components and chip facets. Since the entire optical feedback path is on-chip, the TE polarization of light is preserved. A grating coupler is placed on the other output of the 2 × 2 MMI, from which the power, spectrum, and RIN of the laser can be measured.

First, the RIN is recorded while the QD-DFB bias current is varied from 60 mA to 160 mA in Fig. 6(a). For this measurement, the backreflection is kept to the minimum −30 dB value (VOA on) in order to set the baseline for laser RIN. Next, the RIN of the QD-DFB biased at a typical operating current of 150 mA is measured with the VOA fully on and off. The results in Fig. 6(b) show less than 2 dB/Hz difference in the RIN, suggesting that the laser is not perturbed even at the strongest backreflection level of −13 dB (VOA off). The optical spectrum of the laser in Fig. 6(c) is unchanged between the two conditions, outside of a slight redshift in lasing wavelength due to thermal crosstalk between the laser and the VOA which is driven with 200 mA of current in the "ON" state to achieve the maximum attenuation (lowest backreflection).

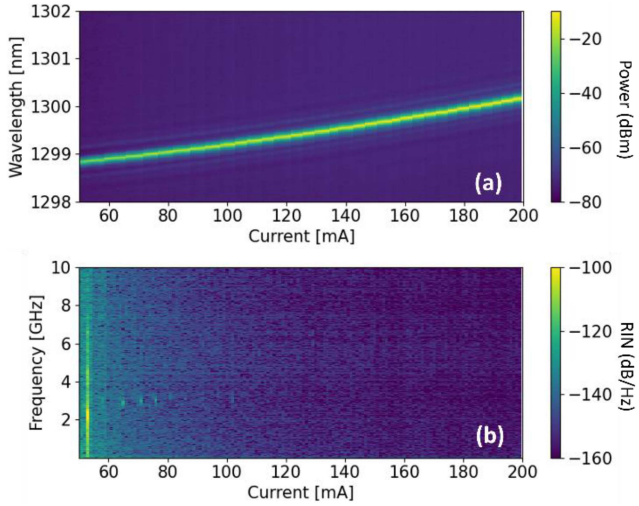


Fig. 7. (a) Optical spectrum and (b) electrical RIN map plotted versus laser bias current up to 200 mA. The VOA attenuation was set to a minimum, resulting in −13.0 dB of optical feedback delivered to the QD-DFB.

Finally, it is important to measure the RIN across a fine sweep of laser bias. Doing so ensures that the relative phase of the reflection with respect to the laser is swept. This is important because the distance of the reflection is roughly 1 cm. This separation is indicative of typical waveguide lengths in a PIC but is not long enough to be in the "long cavity" regime in which the reflection is incoherent and its phase no longer plays a role in the laser feedback dynamics [24]. A fine sweep of laser current ensures that a full range of coherent and incoherent reflections are captured in this feedback experiment. The results are shown in Fig. 7 for the maximum backreflection level of −13 dB. The optical spectrum shows no signs of multi-moding or coherence collapse at any of the tested laser bias currents. The RIN shows some elevated levels and some spikes near 3 GHz frequencies at low laser bias currents but has largely vanished at higher bias currents higher than 80 mA. The RIN spikes at laser bias currents is also periodic with the bias, suggesting that the behavior is a coherent effect. However, this behavior disappears at higher bias currents, and the RIN approaches its floor of <−150 dB/Hz.

### B. Data Transmission Demonstration

The QD-DFB's performance under optical feedback is further tested in a data link using a reverse biased silicon microring modulator (MRM) on another chip which was also fabricated using Intel's Silicon Photonics process [26]. The experimental setup is shown in Fig. 8. The QD-DFB laser in the feedback tolerance testbed in Fig. 5 is biased at 80 mA and the output light is coupled to a single-mode fiber and subsequently pre-amplified by a praseodymium-doped fiber amplifier (PDFA) before being coupled into the MRM chip. The silicon MRM has a radius of 6 um and a Q-factor of 4500. Its phase efficiency and 3 dB electro-optic bandwidth were measured to be 0.46 V·cm and 45 GHz, respectively. The MRM was driven by PAM4 signals using an arbitrary waveform generator (AWG) followed by a RF amplifier at a data rate of 64 Gb/s for NRZ

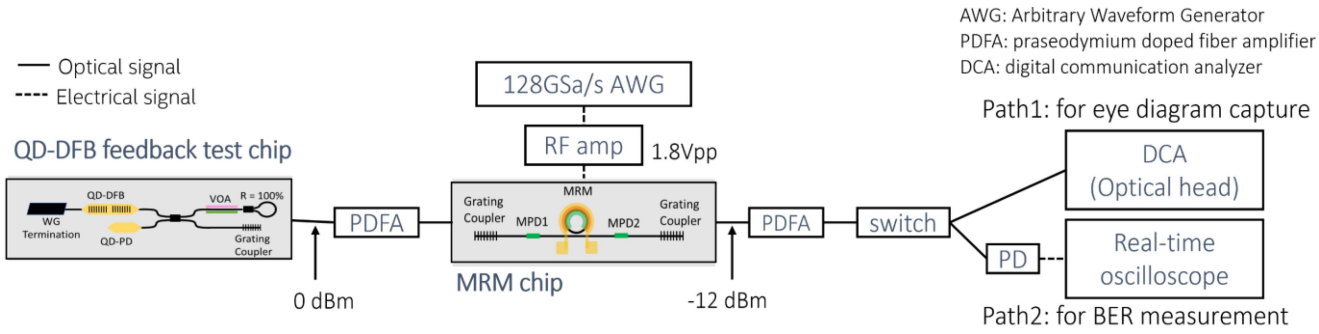


Fig. 8. The experimental setup consisting of two different chips used to demonstrate isolator-free data transmission of the QD-DFB and silicon MRM under varying optical feedback levels.

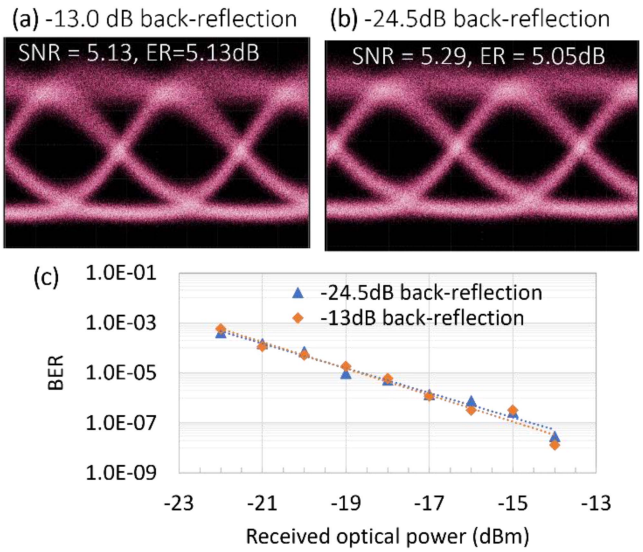


Fig. 9. (a) Measured eye diagram of a 64 Gbps NRZ signal with the QD-DFB at −13.0 dB and (b) −24.5 dB optical backreflection. (c) The BER versus received optical power at the two backreflection levels, showing no measurable differences.

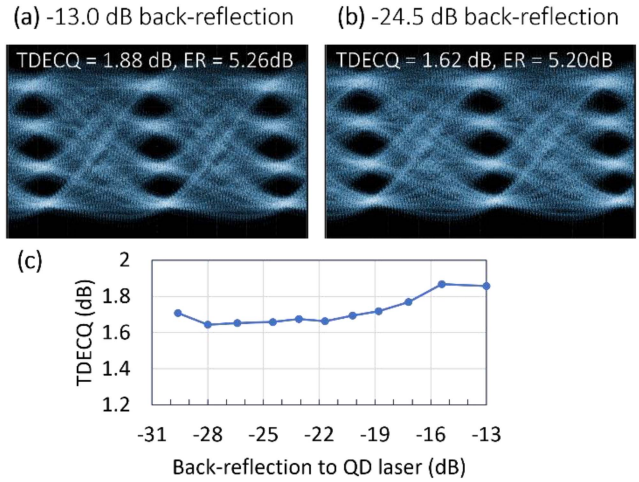


Fig. 10. (a) Measured eye diagram of a 128 Gbps PAM-4 signal with the QD-DFB at −13.0 dB and (b) −24.5 dB optical backreflection. (c) The measured TDECQ versus backreflection levels.

and 128 Gb/s for PAM-4. The modulated optical signal, further amplified by another PDFA, was then either detected by a digital communication analyzer (DCA) for eye diagram measurements or by a high-speed photodiode and then captured by a real-time oscilloscope for bit error rate (BER) measurements. The PDFA are necessary due to the extra loss (∼18 dB) from the multiple grating couplers in the setup, as shown in Fig. 8. Throughout the measurements, the MRM was actively locked to the QD-DFB wavelength at a detuning corresponding to 6 dB insertion loss point. This is achieved by monitoring the power levels before and after the MRM using on-chip monitor photodetectors (MPD). The backreflection back to the QD-DFB is varied using the on-chip VOA as described in the previous section.

For a 64 Gb/s NRZ signal, the recorded eyes are wide-open at all the tested backreflection levels. Two snapshots of the eye diagrams at −13.0 dB and −24.5 dB of reflection are shown in Fig. 9(a) and (b) with extinction ratio (ER) $>$ 5 dB and signal-to-noise ratio (SNR) $>$ 5. Bit error rate (BER) is also measured as a function of received optical power for each case, showing nearly identical behavior (Fig. 9(c)). Similarly, wide-open eye diagrams are measured at all measured backreflection levels for the 128 Gb/s PAM-4 signal as shown in Fig. 10. The TDECQ values are recorded for each backreflection level, and a TDECQ penalty of $<$0.2 dB was measured at the strongest optical feedback level of −13.0 dB. As the feedback strength is decreased beyond −22 dB, the TDECQ value stabilizes at around 1.65 dB, the same value when measured using a reference commercial tunable laser with an optical isolator at the same wavelength and output power as the QD laser. These results demonstrate the feedback tolerance of the QD laser up to −13.0 dB limited by the on-chip test structure.

## V. Conclusion

We demonstrate the first heterogeneous silicon quantum dot lasers integrated on a 300 mm silicon photonics platform. The devices show the desired characteristics of quantum dot lasers including single mode lasing with output powers $>$28 mW, high temperature operation up to 150 °C, and high resiliency to optical backreflections as demonstrated by isolator-free data transmission at 128 Gbps and under −13.0 dB of optical backreflection. The integration of QD lasers with silicon photonics at scale shows great potential to play an important role in both current and future applications such as datacom, telecom, sensing, and AI/ML.

## ACKNOWLEDGMENT

The authors thank Richard Jones, Ranju Venables, Banaful Paul, George Ghiurcan, John Heck, Leo Varghese, Meredith Hanolsy, Yuliya Akulova, Olufemi Dosunmu, and Saeed Fathololoumi, Ling Liao, Kamath Kishore, Amit Nagra, Pooya Tadayon, and James Jaussi for their support and technical guidance.

## REFERENCES

[1] C. Shang et al., "Perspectives on advances in quantum dot lasers and integration with Si photonic integrated circuits," *ACS Photon.*, vol. 8, no. 9, pp. 2555–2566, 2021.

[2] Y. Arakawa and H. Sakaki, "Multidimensional quantum well laser and temperature dependence of its threshold current," *Appl. Phys. Lett.*, vol. 40, no. 11, pp. 939–941, 1982.

[3] D. Bimberg et al., "Quantum dot lasers: Breakthrough in optoelectronics," *Thin Solid Films*, vol. 367, no. 1/2, pp. 235–249, 2000.

[4] J. Duan et al., "1.3- $\mu$m reflection insensitive InAs/GaAs quantum dot lasers directly grown on silicon," *IEEE Photon. Technol. Lett.*, vol. 31, no. 5, pp. 345–348, Mar. 2019.

[5] Z. Zhang, D. Jung, J. C. Norman, W. W. Chow, and J. E. Bowers, "Linewidth enhancement factor in InAs/GaAs quantum dot lasers and its implication in isolator-free and narrow linewidth applications," *IEEE J. Sel. Topics Quantum Electron.*, vol. 25, no. 6, Nov./Dec. 2019, Art. no. 1900509.

[6] B. J. H. Stadler and T. Mizumoto, "Integrated magneto-optical materials and isolators: A review," *IEEE Photon. J.*, vol. 6, no. 1, Feb. 2014, Art. no. 0600215.

[7] D. Huang, P. Pintus, and J. E. Bowers, "Towards heterogeneous integration of optical isolators and circulators with lasers on silicon," *Opt. Mater. Exp.*, vol. 8, pp. 2471–2483, 2018.

[8] C. Shang et al., "Electrically pumped quantum-dot lasers grown on 300 mm patterned Si photonic wafers," *Light. Sci. Appl.*, vol. 11, no. 1, 2022, Art. no. 299.

[9] K. Feng et al., "Quantum dot lasers directly grown on 300 mm Si wafers: Planar and in-pocket," *Photonics*, vol. 10, no. 5, 2023, Art. no. 534.

[10] W. Wei et al., "Monolithic integration of embedded III-V lasers on SOI," *Light. Sci. Appl.*, vol. 12, no. 1, 2023, Art. no. 84.

[11] G. Kurczveil, D. Liang, M. Fiorentino, and R. G. Beausoleil, "Robust hybrid quantum dot laser for integrated silicon photonics," *Opt. Exp.*, vol. 24, no. 14, pp. 16167–16174, 2016.

[12] Y. Wan et al., "High speed evanescent quantum-dot lasers on Si," *Laser Photon. Rev.*, vol. 15, no. 8, 2021, Art. no. 2100057.

[13] R. Jones et al., "Heterogeneously integrated InP/silicon photonics: Fabricating fully functional transceivers," *IEEE Nanotechnol. Mag.*, vol. 13, no. 2, pp. 17–26, Apr. 2019.

[14] R. Blum, "Integrated silicon photonics for high-volume data center applications," *Opt. Interconnects XX*, vol. 11286, pp. 141–149, 2020.

[15] D. Huang et al., "8-channel hybrid III-V/silicon DFB laser array with highly uniform 200 GHz spacing and power," in *Proc. 27th Int. Semicond. Laser Conf.*, 2021, pp. 1–2.

[16] G. Kurczveil, C. Zhang, A. Descos, D. Liang, M. Fiorentino, and R. Beausoleil, "On-chip hybrid silicon quantum dot comb laser with 14 error-free channels," in *Proc. IEEE Int. Semicond. Laser Conf.*, 2018, pp. 1–2.

[17] A. Malik, J. Guo, M. A. Tran, G. Kurczveil, D. Liang, and J. E. Bowers, "Widely tunable, heterogeneously integrated quantum-dot O-band lasers on silicon," *Photon. Res.*, vol. 8, no. 10, pp. 1551–1557, 2020.

[18] C. Xiang et al., "High-performance silicon photonics using heterogeneous integration," *IEEE J. Sel. Topics Quantum Electron.*, vol. 28, no. 3, May/Jun. 2022, Art. no. 8200515.

[19] B. Hakki and T. Paoli, "Gain spectra in GaAs double−Heterostructure injection lasers," *J. Appl. Phys.*, vol. 46, no. 3, pp. 1299–1306, 1975.

[20] T. Septon et al., "Large linewidth reduction in semiconductor lasers based on atom-like gain material," *Optica*, vol. 6, no. 8, pp. 1071–1077, 2019.

[21] J. C. Norman et al., "The importance of p-doping for quantum dot laser on silicon performance," *IEEE J. Quantum Electron.*, vol. 55, no. 6, Dec. 2019, Art. no. 2001111.

[22] W. W. Chow, Z. Zhang, J. C. Norman, S. Liu, and J. E. Bowers, "On quantum-dot lasing at gain peak with linewidth enhancement factor $\alpha_{\mathrm{H}} = 0$," *APL Photon.*, vol. 5, no. 2, 2020, Art. no. 026101.

[23] J. Duan et al., "Dynamic and nonlinear properties of epitaxial quantum dot lasers on silicon for isolator-free integration," *Photon. Res.*, vol. 7, no. 11, pp. 1222–1228, 2019.

[24] L. Coldren, S. Corzine, and M. L. Masanovic, *Diode Lasers and Photonic Integrated Circuits*. Hoboken, NJ, USA: Wiley, 2012.

[25] R. Jones, "Overview and future challenges on III-V integration technologies in silicon photonics platform," in *Proc. 2021 Opt. Fiber Commun. Conf. Exhib.*, 2021, pp. 1–3.

[26] X. Wu et al., "A single-chip high-speed silicon photonic transmitter with integrated laser and micro-ring modulator," in *Proc. IEEE Silicon Photon. Conf.*, 2023, pp. 1–2.